Supporting Information

Drake et al. 10.1073/pnas.1120985109

SI Materials and Methods

Clinical Prostate Tissue Microarrays (TMA). The prostate TMA was constructed as previously described (1). Briefly, 75 prostatectomy specimens from patients never treated with hormonal therapy were reviewed and areas of normal prostate, high-grade prostatic intraepithelial neoplasis (HGPIN), and hormone-naïve prostate cancer (HNPC) were marked for sampling. Tumors ranged from Gleason patterns 2–5. Two to three cores per sample, measuring 0.6 mm in diameter, were obtained from selected regions in each donor paraffin block and transferred to a recipient paraffin block and the resulting block contained a total of 200 cores. A section was obtained from the TMA for H&E staining as quality control and unstained sections were used for immunohistochemical staining.

Another TMA was constructed from transurethral resection tissue blocks from 20 patients who failed hormonal therapy (castration-resistant prostate cancer, CRPC) and developed urinary obstruction. Similarly, two cores were taken from each donor block and transferred to a recipient block. A section was obtained from the TMA for H&E staining as quality control and unstained sections were used for immunohistochemical staining.

Lentiviral Vector Construction. Construction of the plasmids carrying the oncogenes myristoylated AKT (mAKT), AR, AKT-ERG are described previously (2–4). The plasmid 12544 carrying K-RASG12V DNA was purchased from Addgene (5). The ORF of K-RASG12V was amplified by PCR using the following primers: forward primer, 5′-CATCATACTAGTGCCACCatgactgaatataaacttgtggtagttg-3′; and reverse primer, 5′-CATCATGTTACCttacataattacacactttgtctttgacttc-3′. The PCR product was digested with SpeI and HpaI enzyme, whereas the lentiviral vector FUCRW-Cre was digested with the same enzyme that released the Cre gene and generated the lentiviral backbone with SpeI and HpaI cohesive ends. The K-RASG12V fragment was ligated into the lentiviral backbone and is designated as FU-K-RASG12V-CRW.

Prostate Regeneration and Prostate Epithelial Viral Infections. The regeneration process, lentivirus preparation, titering, and infection of dissociated prostate cells were performed as described previously under University of California, Los Angeles (UCLA) safety regulations for lentivirus use (6). Housing, maintenance, and all surgical and experimental procedures were undertaken in compliance with the regulations of the division of Laboratory Animal Medicine of the UCLA. Prostate regeneration was adapted from previous reports (7). Dissociated prostate cell suspension was prepared from 6- to 10-wk-old Bl6 mice. The dissociated cells were infected with lentivirus to generate the following tumors: FU-mAKT-CRW (multiplicity of infection, MOI ~60) for mAKT tumors, FU-mAKT-IRES-ERG-CRW (MOI ~50) for mAKT/ERG tumors, FU-mAKT-CRW (MOI ~40) and FU-AR-CGW (MOI ~40) for mAKT/AR tumors, and FU-mAKT-CGW (MOI ~40) and FU-K-RASG12V-CRW (MOI ~40) for mAKT/K-RASG12V tumors. Infected cells (2×10^5) were mixed with urogenital sinus mesenchyme (UGSM) (2×10^5). Grafts were implanted under the kidney capsule in SCID mice the following morning and allowed to regenerate for 12 wk.

Western Blot and Immunohistochemistry. Tumors were either flash frozen (Western analysis) or fixed in 10% buffered formalin overnight, embedded in paraffin, and sectioned at 4 μm (IHC analysis). For Westerns, equal protein amounts of urea lysates were used from tissues prepared as described in *Quantitative Analysis of Phosphotyrosine Peptides by Mass Spectrometry*. Antibodies were diluted as follows: AKT (1:1,000; Santa Cruz), pAKT S^{473} (1:2,000; Cell Signaling), ERG (1:500; Epitomics), AR (1:1,000; Santa Cruz), K-RAS (1:250; Calbiochem), 4G10 (1:2,500; Millipore), pEGFR Y^{1068} (1:1,000; Cell Signaling), EGFR (1:1,000; Cell Signaling), pPTPN11 Y^{584} (1:1,000; Cell Signaling), PTPN11 (1:1,000; Cell Signaling), pSTAT3 Y^{705} (1:2,000; Cell Signaling), STAT3 (1:1,000; Cell Signaling), pJAK2 $Y^{1007/1008}$ (1:500; Cell Signaling), JAK2 (1:1,000; Cell Signaling), pERK1/2$^{T202/Y204}$ (1:2,000; Cell Signaling), ERK1/2 (1:1,000; Cell Signaling), pPTK2B Y^{402} (1:1,000; Cell Signaling), PTK2B (1:1,000; Cell Signaling), pSRC Y^{416} (1:1,000; Cell Signaling), SRC (1:5,000; Cell Signaling), ABL1 (1:5,000; Witte Laboratory) (8), and pABL1 Y^{245} (1:500; Cell Signaling). ECL substrate (Millipore) was used for detection and development on GE/Amersham film. For IHC, sections were stained with hematoxylin and eosin for representative histology. Tissue sections were heated at 65 °C for 1 h to melt the paraffin followed by rehydration. Antigen retrieval was performed using citric acid buffer and visualization was performed using EnVision$^+$ system (Dako). The same primary antibodies from Western blots were used, unless explicitly stated, and diluted as follows: 4G10 (1:1,000), pSRC Y^{416} (1:50), pSTAT3 Y^{705} (1:200), AKT (1:300; Cell Signaling), AR (1:200), and ERG (1:50). All primary antibodies recognizing tyrosine phosphorylated motifs were diluted in commercial antibody diluent (Cell Signaling).

Quantitative Analysis of Phosphotyrosine Peptides by Mass Spectrometry. The hybridoma was purchased from The Developmental Studies Hybridoma Bank, University of Iowa, and purified antibody (clone 4G10) was then chemically conjugated to protein G beads using dimethyl pimelimidate (DMP) as described (CSH Protocols; doi:10.1101/pdb.prot4303). Phosphotyrosine peptide immunoprecipitation was performed with pan-specific antiphosphotyrosine antibodies (clone 4G10,) using 35 mg of total protein isolated from 300 to 500 mg frozen tumor mass as previously described (9, 10). Phosphorylated peptides were analyzed by liquid chromatography tandem mass spectrometry (LC-MS/MS) using an Eksigent autosampler coupled with Nano2DLC pump (Eksigent) and LTQ-Orbitrap (Thermo Fisher Scientific). The samples were loaded onto an analytical column (10 cm × 75 μm i.d.) packed with 5 μm Integrafit Proteopep2 300 Å C18 (New Objective). Peptides were eluted into the mass spectrometer using a HPLC gradient of 5–40% Buffer B in 45 min followed by a quick gradient of 40–90% Buffer B in 10 min, where Buffer A contains 0.1% formic acid in water and Buffer B contains 0.1% formic acid in acetonitrile. All HPLC solvents were Ultima Gold quality (Fisher Scientific). Mass spectra were collected in positive ion mode using the Orbitrap for parent mass determination and the LTQ for data-dependent MS/MS acquisition of the top five most abundant peptides. Each sample was analyzed twice (replicate runs) and in each run one-half of the sample was injected. MS/MS fragmentation spectra were searched using SEQUEST (version v.27, rev. 12, Thermo Fisher Scientific) against a database containing the combined human-mouse IPI protein database (downloaded December 2006 from ftp.ebi.ac.uk). Search parameters included carbamidomethyl cysteine (*C) as a static modification. Dynamic modifications included phosphorylated tyrosine, serine, or threonine (pY, pS, pT, respectively) and oxidized methionine (*M). Results derived from database searching were filtered using the following criteria: Xcorr >1.0(+1), 1.5 (+2), 2(+3); peptide probability score <0.001; dCn >0.1; and mass accuracy <25 ppm (parts per million) with Bioworks version

3.2 (Thermo Electron). We estimated the false-positive rate of sequence assignments at 0.5% on the basis of a composite target-reversed decoy database search strategy (11). AScore was used to more accurately localize the phosphate on the peptide (12). Peptide peaks sequenced in experimental tumors and control lines but not others were located in the remaining samples by aligning the chromatogram elution profiles using a dynamic time warping algorithm (9, 10). Relative amounts of the same phosphopeptide across samples run together were determined using custom software to integrate the area under the unfragmented (MS1) monoisotopic peptide peak (10, 13). All peaks corresponding to phosphosites were inspected manually and any errors in the automated quantitation were corrected. MS2 spectra for all reported phosphopeptides are available under the PRIDE accession numbers 20879–20889 (14).

Data Analysis. The number of unique phosphorylation sites identified in our experiments was determined by collapsing multiple phosphopeptide ions representing the same phosphorylation site. Multiple detections of the same phosphosite includes phosphopeptides of different ion charge state, modification (e.g., oxidized methionine), and missed trypsin cleavage sites. Multiple detections were compared to ensure no disagreement in trend, and the MS ion with the highest intensity across the samples in an experimental batch was kept as representative for subsequent data analysis. The phosphosite residue numbers listed correspond to the International Protein Index (IPI) accession number in the mouse genome, and any phosphopeptides that did not map to the mouse genome were removed. For clustering, we removed any peptides that had an ANOVA score less than 0.2. Hierarchical clustering was performed using the Cluster program with the Pearson correlation and pairwise complete linkage analysis (15). Java TreeView was used to visualize clustering results (16). Quantitative data for each phosphopeptide can be found in Dataset S1.

Enrichment Analysis of Kinase Activity. Permutation analysis was performed by randomly shuffling the peptide ranked list, followed by calculation of the Kolmogorov–Smirnov statistic for this permutation. After 1,000 permutations, the fraction of randomly ranked lists resulting in a Kolmogorov–Smirnov statistic greater than or equal to the observed value was defined as the permutation-based frequency of random occurrence (i.e., the permutation-based P value). To normalize for the different number of predictions for each upstream kinase, we calculated the normalized Kolmogorov–Smirnov score by dividing the observed enrichment score by the mean of the absolute value of all permutation enrichment scores.

1. Huang J, et al. (2005) Differential expression of interleukin-8 and its receptors in the neuroendocrine and non-neuroendocrine compartments of prostate cancer. *Am J Pathol* 166:1807–1815.
2. Xin L, Lawson DA, Witte ON (2005) The Sca-1 cell surface marker enriches for a prostate-regenerating cell subpopulation that can initiate prostate tumorigenesis. *Proc Natl Acad Sci USA* 102:6942–6947.
3. Zong Y, et al. (2009) ETS family transcription factors collaborate with alternative signaling pathways to induce carcinoma from adult murine prostate cells. *Proc Natl Acad Sci USA* 106:12465–12470.
4. Xin L, et al. (2006) Progression of prostate cancer by synergy of AKT with genotropic and nongenotropic actions of the androgen receptor. *Proc Natl Acad Sci USA* 103: 7789–7794.
5. Khosravi-Far R, et al. (1996) Oncogenic Ras activation of Raf/mitogen-activated protein kinase-independent pathways is sufficient to cause tumorigenic transformation. *Mol Cell Biol* 16:3923–3933.
6. Xin L, Ide H, Kim Y, Dubey P, Witte ON (2003) In vivo regeneration of murine prostate from dissociated cell populations of postnatal epithelia and urogenital sinus mesenchyme. *Proc Natl Acad Sci USA* 100(Suppl 1):11896–11903.
7. Lukacs RU, Goldstein AS, Lawson DA, Cheng D, Witte ON (2010) Isolation, cultivation and characterization of adult murine prostate stem cells. *Nat Protoc* 5:702–713.
8. Schiff-Maker L, et al. (1986) Monoclonal antibodies specific for v-abl- and c-abl-encoded molecules. *J Virol* 57:1182–1186.
9. Rubbi L, et al. (2011) Global phosphoproteomics reveals crosstalk between Bcr-Abl and negative feedback mechanisms controlling Src signaling. *Sci Signal* 4:ra18.
10. Skaggs BJ, et al. (2006) Phosphorylation of the ATP-binding loop directs oncogenicity of drug-resistant BCR-ABL mutants. *Proc Natl Acad Sci USA* 103:19466–19471.
11. Elias JE, Haas W, Faherty BK, Gygi SP (2005) Comparative evaluation of mass spectrometry platforms used in large-scale proteomics investigations. *Nat Methods* 2: 667–675.
12. Beausoleil SA, Villén J, Gerber SA, Rush J, Gygi SP (2006) A probability-based approach for high-throughput protein phosphorylation analysis and site localization. *Nat Biotechnol* 24:1285–1292.
13. Zimman A, et al. (2010) Activation of aortic endothelial cells by oxidized phospholipids: A phosphoproteomic analysis. *J Proteome Res* 9:2812–2824.
14. Vizcaíno JA, et al. (2010) The Proteomics Identifications database: 2010 update. *Nucleic Acids Res* 38(Database issue):D736–D742.
15. Eisen MB, Spellman PT, Brown PO, Botstein D (1998) Cluster analysis and display of genome-wide expression patterns. *Proc Natl Acad Sci USA* 95:14863–14868.
16. Saldanha AJ (2004) Java Treeview—extensible visualization of microarray data. *Bioinformatics* 20:3246–3248.

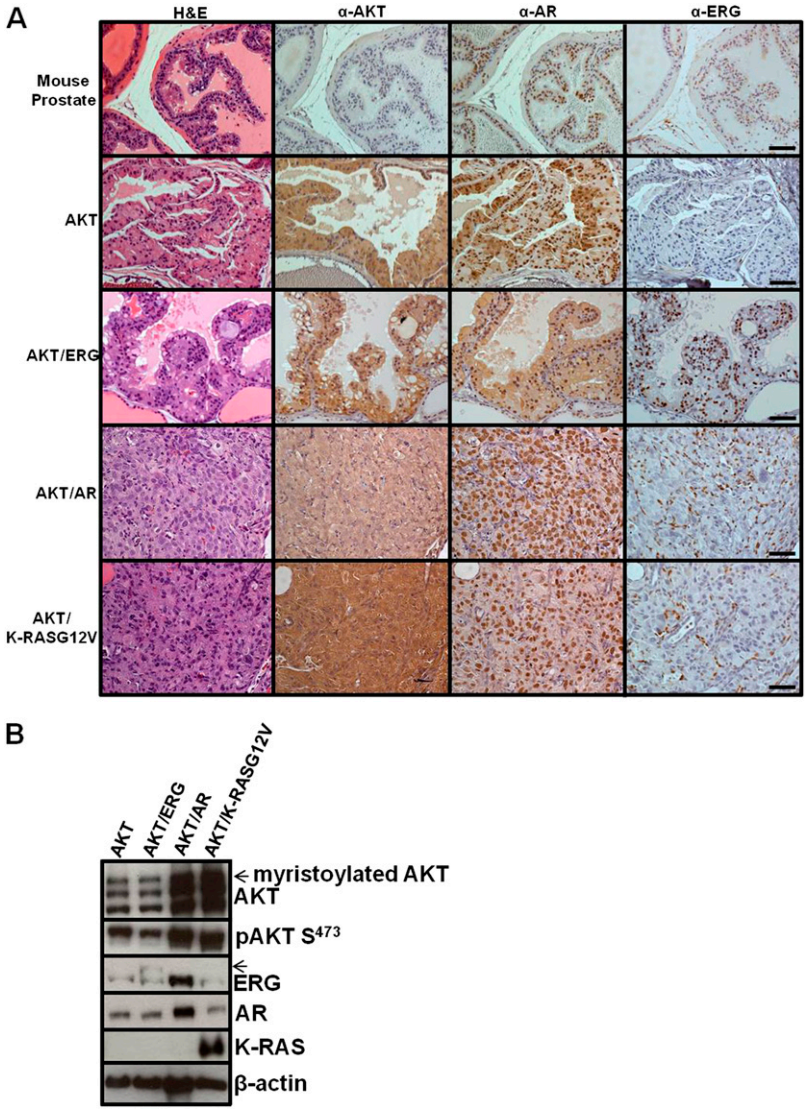

Fig. S1. Confirmation of oncogene expression in mouse tumors. (*A*) Immunohistochemical staining for AKT, androgen receptor (AR), and ERG show expression of these proteins in the respective tumors investigated. ERG staining can also localize to endogenous endothelial cells as shown in AKT/AR and AKT/K-RASG12V tumors. (*B*) Western blot analysis confirms the expression of each oncogene after lentiviral transduction and tumor formation. Arrows, myristoylated AKT expression is shown at the higher molecular weight. ERG expression from the lentiviral vector. ERG expression at the lower molecular weight is from other cells within the tissue (e.g., endothelial cells). (Scale bars, 50 μm.)

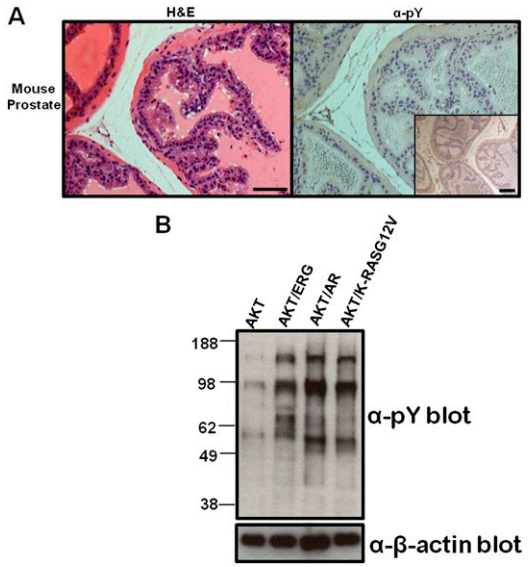

Fig. S2. Analysis of tyrosine phosphorylation in mouse prostate and tumors. (*A*) IHC analysis reveals little tyrosine phosphorylation in normal mouse prostate, similar to what is observed in indolent prostate cancer. (*B*) Western blot analysis using the phosphotyrosine-specific antibody 4G10 reveals increased levels of phosphorylation in the more aggressive tumors. (Scale bars, 50 μm; *Inset*, 100 μm.)

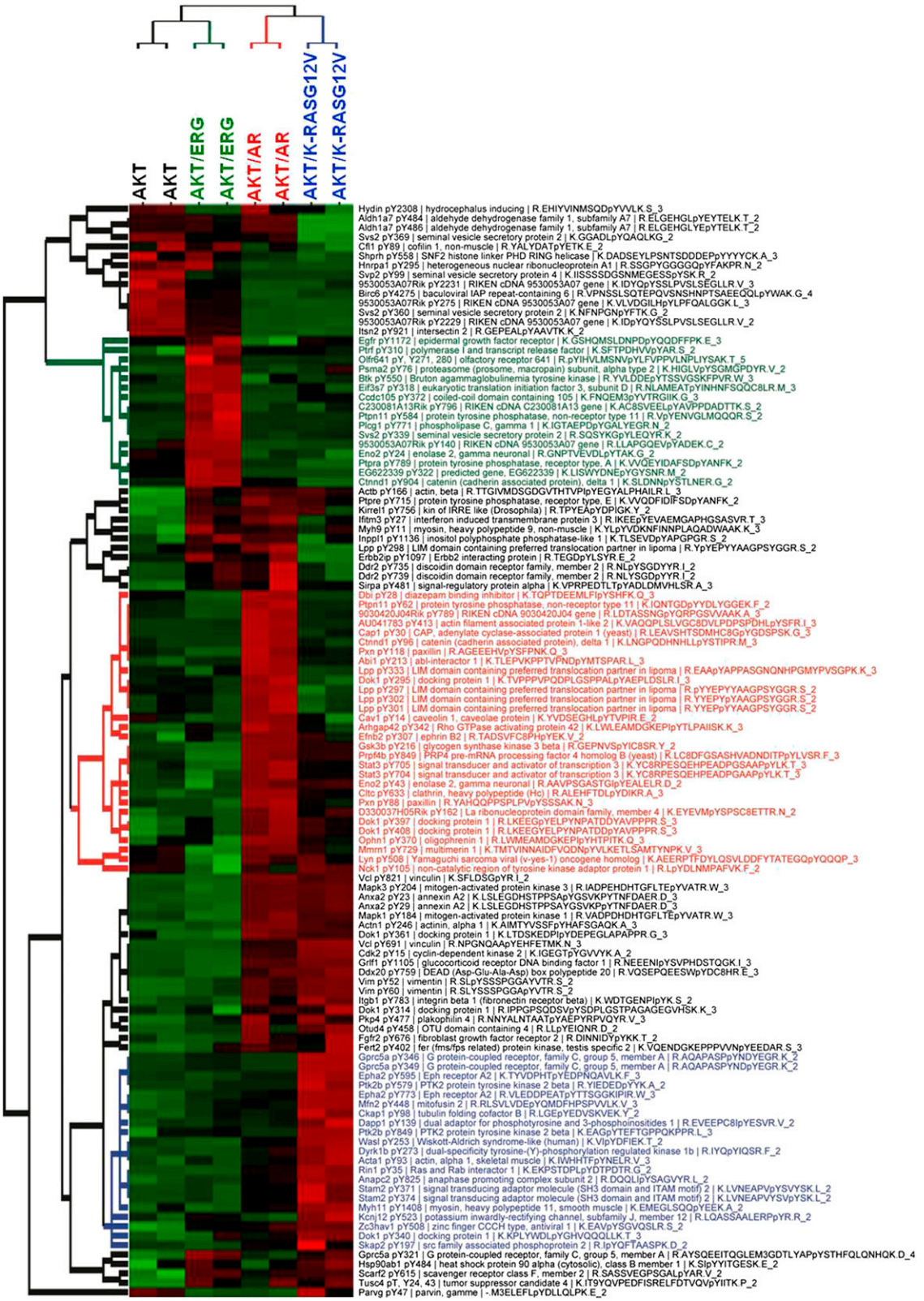

Fig. S3. Global quantitative phosphoprofiling of prostate cancer progression reveals phosphorylation events with distinct oncogene-specific profiles. The phosphoprofiling heatmap of Fig. 4*A* with the protein and residue identities of the phosphorylation events are listed. Gene symbol, phosphosite residue number; Entrez gene product name, phosphopeptide (charge state of mass spectrometry ion).

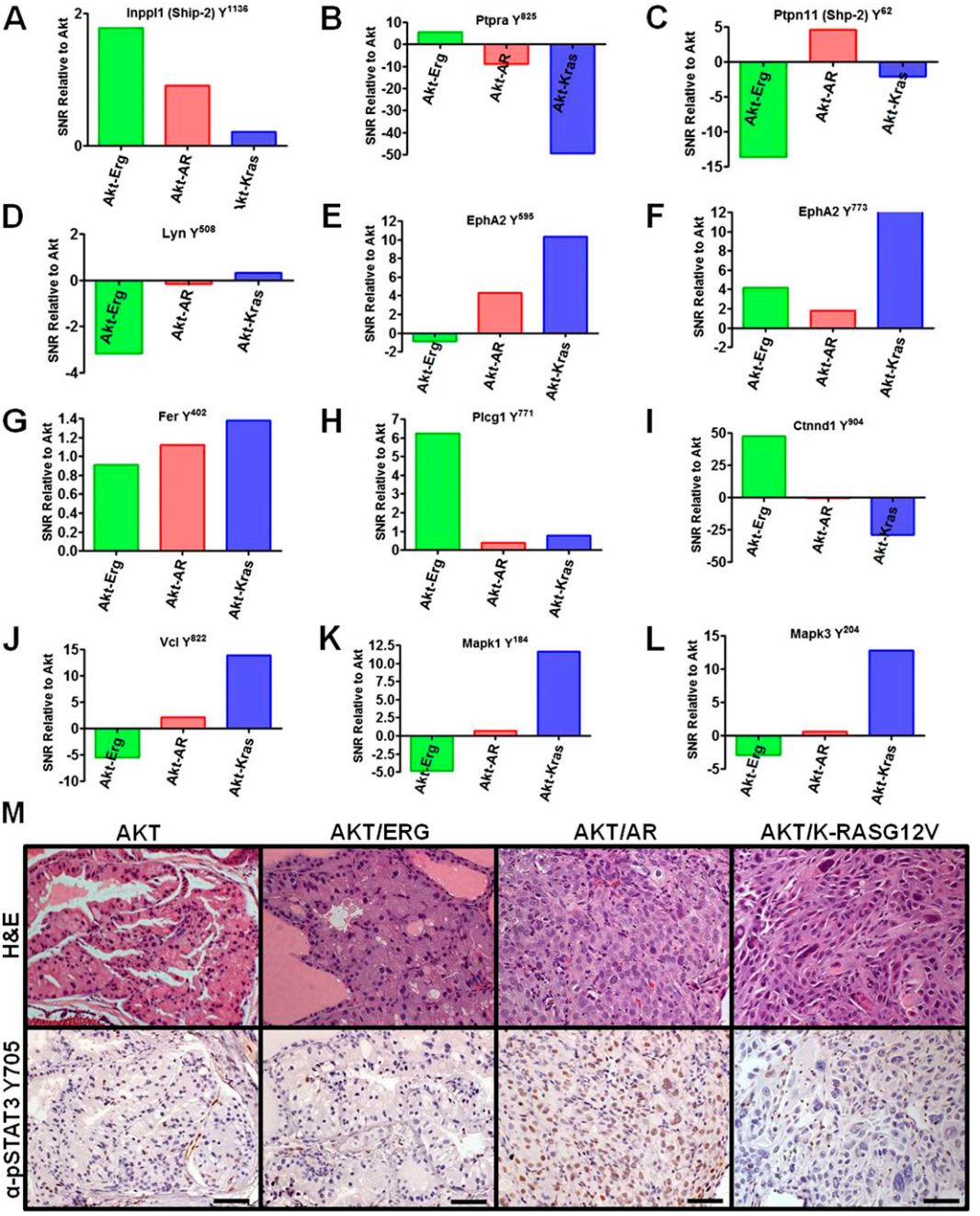

Fig. S4. Identification of activated tyrosine kinases in non-tyrosine kinase-driven prostate tumors. (*A–L*) Relative abundance of phosphopeptide levels of tyrosine kinases, substrates, and phosphatases during progression of prostate cancer. Signal-to-noise ratio (SNR) (relative to AKT) was calculated for each phosphopeptide and plotted. Data from the full phosphoprofiling dataset are depicted in Fig. 4*A*. (*M*) Immunohistochemical staining for tyrosine phosphorylated STAT3 (pSTAT3 Y^{705}) reveals tumor-specific activation of this particular phosphorylation event. (Scale bars, 50 μm.)

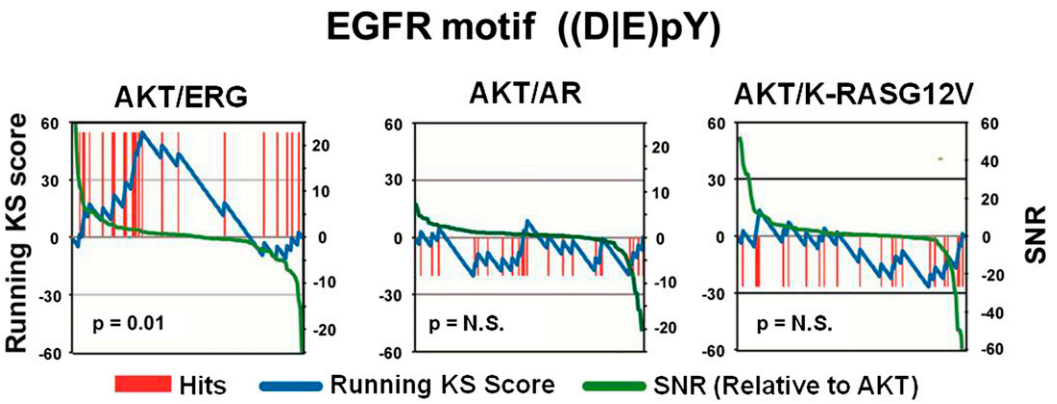

Fig. S5. Enrichment of EGFR target substrates in AKT/ERG tumors. A statistical analysis of tyrosine phosphorylated motifs reveals an enrichment of phosphopeptides of the tyrosine kinase EGFR in AKT/ERG tumors. No significant enrichment of these phosphopeptides was observed in either AKT/AR or AKT/K-RASG12V tumors. Enrichment scores for all kinase motifs are shown in Dataset S2.

Other Supporting Information Files

Dataset S1 (XLSX)
Dataset S2 (XLSX)